

CO in the Bipolar-Radio-Continuum Galaxy NGC 3367

J. A. García-Barreto¹, N.Z. Scoville², J.Koda², & K. Sheth²

Received _____; accepted _____

revised AJ version: Aug 12, 2004

arXiv:astro-ph/0409486v1 20 Sep 2004

¹Instituto de Astronomía, Universidad Nacional Autónoma de México, Apdo Postal 70-264, México D.F. 04510, México; tony@astrocu.unam.mx

²Caltech, Radio Astronomy Millimeter Group, 1200 E. California Blvd, MS 105-24, Pasadena, California 91125, USA

ABSTRACT

CO(1-0) emission has been imaged at $2''$ resolution in the central 10 kpc of the barred spiral galaxy NGC 3367. This galaxy has bipolar synchrotron lobes out to a radii of 6 kpc, straddling the compact nucleus. The peak molecular emission is in a source of radius $2''$ (425 pc) centered on the galaxy nucleus. The molecular gas mass is $\sim 3 \times 10^8 M_\odot$ in this peak and $\sim 5.9 \times 10^8 M_\odot$ within a radius of $4.5''$ (950 pc). The very large gas masses in the central source imply extinctions sufficiently high to completely obscure optical emission lines (e.g. BLR) associated with the nuclear radio source. The observed Balmer lines probably originate in the narrow line region few hundred pc from the nucleus. The CO emission in the central region is elongated NE - SW, very similar to the position angle of the large-scale synchrotron lobes. This elongation is likely due to the non-axisymmetric gravitational potential of the stellar bar. We infer that the NE radio continuum lobe is on the far side of the galaxy and the SW lobe is on the near side. The central mass of molecular gas is sufficient mass to power the AGN accretion luminosity for over 10^8 yrs at $3 M_\odot \text{ yr}^{-1}$.

Subject headings: galaxies: structure — galaxies: spiral — galaxies: individual (NGC 3367) — ISM: molecules

1. INTRODUCTION

Multiwavelength imaging and spectroscopy are vital to understanding the feeding and observed characteristics of active galactic nuclei (AGN). Observations of the molecular gas using the CO (J=1-0) emission line are especially important since this gas may be the fuel for the AGN. The CO (J=1-0) emission peaks toward the centers of most spiral galaxies (Sakamoto et al. 1999b) and the associated interstellar dust and its extinction often determine the emergent optical-UV spectrum of the AGN. In the optical, galactic nuclei are classified according to the width of Balmer lines, emission of high ionization atoms and the ratios of permitted to forbidden emission lines; in the radio continuum, the activity can manifest as central triple sources (Colbert et al. 1996, Ho & Ulvestad 2001, Wilson & Ulvestad 1987, Crane & van der Hulst 1992) or circumnuclear radio continuum structures (e.g. NGC 1326 García-Barreto et al. 1991a, NGC 4314 García-Barreto et al. 1991b).

NGC 3367 (at 43.6 Mpc) is a barred spiral (SBc) galaxy showing a remarkable triple radio continuum synchrotron structure: a central unresolved ($d \leq 65$ pc) source and two larger lobes straddling the nucleus at a radius of about 6 kpc projected on the sky (García-Barreto et al. 1998, García-Barreto, Franco & Rudnick 2002). It also shows an unresolved $H\alpha + N[II]$ central source (diameter $\leq 5''$ or ≤ 1 kpc). It has a modest far infrared luminosity $L_{FIR} \sim 2 \times 10^{10} L_{\odot}$ (Soifer et al. 1989) and is a source of X-ray emission with $L_X \sim 9 \times 10^{40}$ ergs s^{-1} (Fabbiano, Kim & Trinchieri 1992). Optically, it is classified as a weak Liner or HII nucleus (Véron-Cetty & Véron 1986, Ho, Filippenko & Sargent 1995, Véron, Goncalves & Véron-Cetty 1997, Ho, Filippenko & Sargent 1997). The triple synchrotron source suggests that there must be an AGN and the interstellar medium (ISM) may exhibit the effects of this energy release from the central AGN. The orientation of the central synchrotron source and the two lobes at $PA \sim 35^{\circ}$ (see Fig. 11 this paper or Fig. 3 García-Barreto et al. 1998) indicate that the radio jet outflow is not strictly parallel to the rotation axis of the galaxy disk ($PA \sim 140^{\circ}$ for the kinematical minor axis Garcia-Barreto & Rosado 2001).

The HI gas mass for NGC3367 is $\sim 7 \times 10^9 M_{\odot}$ (Huchtmeier & Richter 1989). No previous observations of the molecular gas have been reported; however, from the CO-FIR correlation (Young et al. 1986) one expects a total molecular gas of $\sim 1.6 \times 10^9 M_{\odot}$. $H\alpha$ images show emission from the disk of the galaxy, indicating several regions of massive OB star formation in the disk (García-Barreto et al. 1998, Garcia-Barreto & Rosado 2001). CO interferometric observations of spiral galaxies have indicated higher concentrations of molecular gas in the centers of barred spirals as compared to normal spiral galaxies, supporting the idea of bar-driven gas transport (Sakamoto et al. 1999a, Sakamoto et al. 1999b, Sakamoto, Baker & Scoville 2000, Koda et al. 2002, Sheth et al. 2002, Sheth et al. 2004).

In this paper we report CO(1-0) interferometric mapping of NGC 3367. The images reveal a central molecular gas concentration with radius $4.5''$ (or 0.9 kpc) and mass $\sim 5.9 \times 10^8 M_{\odot}$. This gas concentration is unresolved at our highest CO angular resolution ($2.6 \times 1.9''$ or 550 pc \times 400 pc), suggesting that $H\alpha$, CO and plasma (non-thermal and thermal) are co-extensive in the central 450 pc. The CO is elongated in a SW - NE direction parallel to the radio continuum emission. The morphology of the synchrotron emission suggests a connection between the central source and the large scale radio lobes; however, the CO gas is very likely in the disk of the galaxy while the radio lobes are likely to be above and below the galaxy disk. In §2 we describe the observations; results are presented

in §3; analysis and discussion are presented in §4; finally conclusions are presented in §5.

2. OBSERVATIONS

The central disk of NGC 3367 was observed using the Owens Valley Millimeter Array (Scoville et al. 1993) in the CO (1-0) transition in 4 antennae configurations (C, L, E, H) from 2003 September to 2003 December. The array consists of six 10.4 m radio telescopes and the baselines ranged from 20 to 242 m. The synthesized beams (FWHM) were $4''.2 \times 2''.7$ (natural weighting) and $2''.6 \times 1''.9$ (uniform weighting). Spectral resolution was provided by a digital correlator configured to $128 \times 2\text{MHz}$ (5.2 km s^{-1} resolution). The nearby quasar 1058+015 (2.54 Jy at 115 GHz) was used to calibrate the phase and gain variations. Twenty channel maps, each of 15.6 km s^{-1} width, were cleaned and then combined for the moment maps. Our 1σ rms detection was $0.15 \text{ Jy/km s}^{-1}$ (uniform weighting) and 0.2 Jy/km s^{-1} (natural weighting).

3. RESULTS

Figure 1 shows the interferometric spectrum integrated over the central $17.5''$ (~ 1.8 kpc) from the natural weighting data (fwhm $4''.2 \times 2''.7$). The CO (1-0) channel maps in 15.9 km s^{-1} bins is shown in Figure 2 superimposed on an I-band image (centered at 8040 \AA). CO emission is detected most strongly in the central region of the galaxy – a compact source with elongated to the eastern and western sides (perhaps along the dust lanes in the stellar bar); weaker CO emission is also seen associated with the spiral arm on the east side of the stellar bar and from the western end of the stellar bar. At the last position there is no radio continuum synchrotron emission (see Fig. 6 of García-Barreto et al. 1998) but there is a weak $\text{H}\alpha + \text{N}[\text{II}]$ emission feature (see Fig. 5 of García-Barreto et al. 1998).

3.1. The Nuclear Region

Figures 3 and 4 shows the total CO line flux integrated over 300 km s^{-1} , superposed on the $\text{H}\alpha + [\text{NII}]$ (continuum subtracted) and I band images (García-Barreto, Franco & Carrillo 1996, García-Barreto et al. 1996b). The strongest CO emission (65σ) arises at the compact nucleus and from a circumnuclear structure (see below). The peak intensity of the central emission, in the natural weighting spectrum, is about 250 mJy and the velocity width is 80 km s^{-1} (FWHM). The azimuthally averaged radial distribution of the CO indicates a radius (out to our detection threshold) of $\sim 7''$ (1.5 kpc). A similar, unresolved CO structure was detected in the center of NGC 3368 (SAB(rs)ab, Sakamoto et al. 1999a). The deconvolved size of the central source extent is $525 \text{ pc} \times 300 \text{ pc}$.

3.2. CO and Radio Synchrotron Emission

Figure 5 shows a zoomed image of the central CO concentration from the high resolution image. The *unresolved*, peak emission is at $\alpha(J2000) = 10^h46^m34^s.948$, $\delta(J2000) = +13^\circ45'02.7''$. This position agrees closely with the peak of the synchrotron radio continuum emission ($\alpha(J2000) = 10^h46^m34^s.956$, $\delta(J2000) = +13^\circ45'02.94''$ [García-Barreto, Franco & Rudnick 2002]). A secondary peak occurs to the SW at $\alpha = 34^s.66$; $\delta = 45'00.90''$. The 20-cm radio continuum from the central region has an extension towards PA $\sim 225^\circ$ connecting to the southwest lobe (see Figs. 11 and 12). This is very similar to the PA of the secondary CO peak; however no radio synchrotron emission was actually detected at the secondary CO peak and it is likely that the radio jet is above the galactic disk at this radius.

3.3. CO in the Bar and Disk

Extended CO emission is detected in the central region of NGC 3367 at PA NE - SW, along the center of the stellar bar. Weak extended emission is observed in the CO velocity maps from the west side of disk (blue shifted at 3006 km s^{-1} to 3054 km s^{-1} , see Fig. 2). Those are the expected locations of the leading edge dust lanes from a bar rotating in the counter-clockwise direction (assuming trailing spiral arms).

The north-south structure on the western side of the galaxy is detected at 5σ (Figs. 3 and 4); all of the other extra-nuclear emission features are less than 5σ ($1\sigma = 200 \text{ mJy km s}^{-1}$). Careful examination of the optical *I* band photometry and the CO contours (Figs. 3 and 4) indicates that only the weak, unresolved source in the western side of the disk could be associated with the stellar bar; the north-south CO structure on the west side is most likely not related to the stellar bar. The N-S CO structure is probably associated with an $\text{H}\alpha$ emission region (Fig. 3).

3.4. Gas Kinematics and Dynamical Mass

Figure 6 shows the CO centroid velocities in contours superposed on the integrated CO image in grayscale. The systemic velocity of the galaxy is $\sim 3032 \text{ km s}^{-1}$ from $\text{H}\alpha$ Fabry-Perot (García-Barreto & Rosado 2001). The red shifted gas lies to the NE and the blue shifted gas to the SW. This polarity is the same as that seen in $\text{H}\alpha$ Fabry Perot observations at larger distances from the nucleus – the NE side receding; the SW approaching. The PA of the receding semi major axis (from $\text{H}\alpha$ Fabry Perot) is 51° (García-Barreto & Rosado 2001), indicating that the northwest is the near side of the galaxy (assuming trailing spiral arms). For circular rotation, the contour at the systemic velocity should be a straight line at PA= 140° ; instead, the contour at 3038 km s^{-1} (Fig. 6) is clearly curved. This twisting of the constant velocity contours is commonly seen in barred spiral galaxies, due to the non-circular motions associated with highly eccentric orbits.

The velocity dispersion (2nd moment) map is shown in Figure 7, derived from the naturally weighted map. Average velocity dispersions are $\sigma_v \sim 15 \text{ km s}^{-1}$; however, two regions show extraordinarily large dispersions : at PA $\sim -40^\circ$ (corresponding to the

kinematic minor axis) where $\sigma_v \sim 40 \text{ km s}^{-1}$ and southwest of the nucleus where the dispersion reaches 75 km s^{-1} ($\alpha = 34^{\text{s}}.66; \delta = 45'00''.90$). The latter region is particularly bright in the CO integrated intensity map (Fig. 5) and corresponds to a location where there is very weak synchrotron emission (see Fig. 2 in García-Barreto, Franco & Rudnick 2002).

Figure 8 shows a position-velocity (PV) diagram from the central region along the major axis (PA = 51°) of the galaxy. The total velocity dispersion at the center is nearly 130 km s^{-1} . The blue peak in Figure 8 is at 3022 km s^{-1} and the red shifted peak is at 3068 km s^{-1} . The peaks arise from positions about 50 to 60 pc from the central maximum of the CO integrated emission. If the gas were rotating on the plane of the disk of the galaxy (at $r \sim 175 \text{ pc}$ or $0''.8$ from the center) at about $65 \text{ km s}^{-1} / [\sin(i)] = 130 \text{ km s}^{-1}$, the implied dynamical mass would be $M_{\text{dyn}} \sim RV^2/G = 7 \times 10^8 M_\odot$ (assuming $i \sim 30^\circ$, Garcia-Barreto & Rosado 2001). This dynamical mass is low compared to similar estimates at $R \leq 500 \text{ pc}$ for other barred galaxies (For type SAB's, Sakamoto et al. 1999b find only 1 out of 17 having equivalently low dynamical mass.)

4. DISCUSSION

4.1. Molecular Gas Mass

From the integrated CO line fluxes we have estimated the molecular gas mass in central regions of NGC 3367 using the a standard Galactic conversion factor ($\alpha_{\text{Gal}} = 4M_\odot (\text{K km s}^{-1}\text{pc}^2)^{-1}$ [Young & Scoville 1982]). The molecular gas mass $M(\text{H}_2)$, in units of solar masses, is then obtained using $M(\text{H}_2) = 1.5 \times 10^4 (D_{\text{Mpc}})^2 S_{\text{CO}} (\alpha / (\alpha_{\text{Gal}})) (\text{Jy km s}^{-1})$, including a factor of 1.36 to account for He within the molecular gas (Sakamoto et al. 1999a).

It is of course possible that the standard Galactic CO-to- H_2 conversion factor is not appropriate to the central region of NGC 3367 where there could be a starburst and the physical conditions would be different from those in a Galactic GMC. CO is optically thick and the conversion factor is roughly proportional to $\langle n_{\text{H}_2} \rangle^{1/2} / T_{\text{ex}}$ (Downes, Solomon & Radford 1993, Scoville, Yun & Bryant 1997). To some extent, the density and temperature dependences are likely to offset each other since where the gas density is high, there will be elevated star formation rates and higher temperatures. Our observations only involve one transition; we therefore have no constraints on the CO excitation, and thus adopt the Galactic α .

From the high resolution map (Fig. 5), the peak has a deconvolved size of $2''.5 \times 1''.45$ ($525 \text{ pc} \times 300 \text{ pc}$), an intensity of 11 Jy km s^{-1} , implying a molecular gas mass $3 \times 10^8 M_\odot$. The central CO emission, from the low resolution map (Figs. 3 and 4), is slightly resolved and elongated. The molecular mass estimate within a radius of $4''.5$ (950 pc) is $5.9 \times 10^8 M_\odot$. Lastly, using the total flux in the naturally weighted map out to a radius of $27''$ (5.7 kpc), we obtain $2.6 \times 10^9 M_\odot$. This last estimate is a lower limit to the total gas mass in the galaxy since the interferometer will resolve out extended spatially components.

Sakamoto et al. 1999b observed the central regions of a sample of 20 spiral galaxies

and found a range for $M(H_2)$ of $3.3 \times 10^7 M_\odot$ to $8.1 \times 10^8 M_\odot$ inside 500 pc radius. Average molecular masses inside a radius of 500 pc as a function of galaxy type are: $4.9 \times 10^8 M_\odot$ for SB+SAB galaxies; $2.1 \times 10^8 M_\odot$ for SA; $3 \times 10^8 M_\odot$ for HII galaxies; $3.3 \times 10^8 M_\odot$ for transition galaxies and $3.4 \times 10^8 M_\odot$ for Seyfert galaxies (Sakamoto et al. 1999b). Thus the molecular gas mass for the central region of NGC 3367, $5.9 \times 10^8 M_\odot$, is very similar to that of HII and transition spiral galaxies but it is high for a Hubble type SBc galaxy (Sakamoto et al. 1999b).

4.2. Obscured Optical Emission from the Compact Nucleus

The molecular gas surface density is $\Sigma(H_2) = 2.5 \times 10^3 M_\odot \text{ pc}^{-2}$ at the peak (within $525 \text{ pc} \times 300 \text{ pc}$) and $210 M_\odot \text{ pc}^{-2}$ for the central 1.9 kpc region. For comparison, the surface density is $1500 M_\odot \text{ pc}^{-2}$ inside $715 \times 1600 \text{ pc}$ in NGC 1530 (Downes et al. 1996). And in two early type SBa galaxies with circumnuclear rings (NGC 1326 and NGC 4314), $\Sigma(H_2) = 580 M_\odot \text{ pc}^{-2}$ and $500 M_\odot \text{ pc}^{-2}$ respectively (García-Barreto et al. 1991a, García-Barreto et al. 1991b).

The high value of $\Sigma(H_2)$ ($2.5 \times 10^3 M_\odot \text{ pc}^{-2}$ within $262 \times 150 \text{ pc}$ in NGC 3367) is equivalent to an average column density of $\sim 1.5 \times 10^{23} \text{ cm}^{-2}$. This gas column translates into a visual extinction towards the compact nucleus of $\sim 150 \text{ mag}$ (using $N(H_2)/A_v = 0.94 \times 10^{21} \text{ cm}^{-2} \text{ mag}^{-1}$, Young & Scoville 1982). On the other hand, optical spectra of NGC 3367 show moderately broad $H\alpha + [NII]$ line emission with FWHM velocities up to 600 km s^{-1} . The $H\beta$ line intensity is about twice that of the $[O III] \lambda 5007$ line and there are possible Helium lines ($\lambda 4686$) indicative of W-R stars (Véron-Cetty & Véron 1986, Ho, Filippenko & Sargent 1995). The high extinction associated with the molecular gas would heavily obscure any $H\alpha$ emission from the compact nucleus, suggesting that the observed $H\alpha$ emission must originate from the ionized gas in the narrow line region outside the dense molecular gas. The large dust opacity would explain the lack of wide Balmer lines. The observed optical spectrum from NGC 3367 (Véron-Cetty & Véron 1986, Ho, Filippenko & Sargent 1995, Véron-Cetty & Véron 1996) is consistent with the ionized gas emission lines arising from the surfaces of the molecular clouds.

4.3. The Nuclear Gas Distribution

The high resolution CO map of the central region (Figs. 3, 4, 5) indicates a very striking distribution of the molecular gas as compared to the radio continuum distribution. The CO maps show extended emission to the west and east near extensions in the radio continuum synchrotron (see Figs. 10 and 11). The PV diagram (Fig. 8) shows two peaks along the major axis at different velocities. There are several possible explanations for these two peaks in the CO, straddling the nucleus : (a) a central hole in the gas, (b) an increase in the line broadening on the nucleus or (c) a decrease in the CO emissivity due to extreme physical conditions there.

In the case of NGC 3367 there is additionally a plasma outflow from the AGN which might clear gas from the vicinity of the AGN. The orientation of the synchrotron triple sources and the plasma outflow is likely to be perpendicular to the accretion disk – and

both are apparently inclined with respect to the galaxy disk (Pringle et al. 1999, Kinney et al. 2000). It is unlikely that the outflowing plasma is directed by interaction with the dense molecular gas (Henriksen, Vallée & Bridle 1981, Bridle & Perley 1984, Blandford 1990). Molecular gas to the NE ($\alpha = 35^m.15$; $\delta = 45'03''$) is in a region of no detectable radio emission (in fact the radio continuum synchrotron emission shows a sharp cutoff [see Figs. 10 and 11]). The kinetic energy required to significantly displace the molecular gas in the west source is $\sim 1/2mv^2 \simeq 2 \times 10^{52}$ ergs, assuming a velocity of about 15 km s^{-1} and a mass of about $10^7 M_\odot$.

Based on the available observations (optical red continuum, $H\alpha$, radio continuum synchrotron, CO(1-0)), we favor the interpretation that the central density of molecular gas is reduced compared to that at $\sim 100 \text{ pc}$. NGC 1068 is another spiral galaxy with bipolar synchrotron lobes (although smaller in extent, only $\sim 450 \text{ pc}$). High angular resolution CO(1-0) and CO(2-1) interferometry of NGC 1068 reveals two concentrations molecular gas straddling the compact nucleus at a PA perpendicular to that of the plasma outflow within 100 pc (Schinnerer et al. 2000). In the case of NGC 1068, Schinnerer *et al.* suggest a model with the molecular gas in a warped disk of thickness 10 pc and a radius of about 150 pc . The BLR in NGC 1068 would be obscured to our line-of-sight; however, optical polarization studies do indicate its existence in broad polarized line wings on the $H\alpha$ emission (Antonucci & Miller 1985).

4.4. Gas Flow to the Nucleus

In barred spiral galaxies, exchange of angular momentum of bar and gas (molecular clouds) cause gas flow inwards from the corotation radius (CR) to the inner Lindblad resonance, forming a circumnuclear structure or ring (Buta 1986, Buta & Combes 1996). Gas should also be driven outwards from CR to the outer Lindblad resonance (OLR). Inside the CR, the gas moves on x_1 orbits elongated parallel to the bar and on x_2 orbits perpendicular to the bar (Contopoulos & Grosbøl 1989). Near the ILR the orbits change from x_1 to x_2 ; viscous dissipation forces a continuous change between the two families of orbits and shocks can result. Barred galaxies like NGC 1530 (SBb) shows CO gas from the central region [$M(\text{H}_2) = 6 \times 10^9 M_\odot$] as well as from along the dust lanes along the bar (Reynaud & Downes 1997, Reynaud & Downes 1998). On the other hand, barred galaxies like NGC 4314 (García-Barreto et al. 1991b, Regan, Sheth & Vogel 1999) or NGC 5383, show no molecular gas in the dust lanes except where the dust lanes join the nuclear circumnuclear structure (Regan, Sheth & Vogel 1999).

As stated earlier, the amount of total mass ($M(\text{HI}) + M(\text{H}_2)$) is about $9 \times 10^9 M_\odot$ in NGC 3367, which is similar to the amount of mass found in other spiral galaxies (Sakamoto et al. 1999a, Sakamoto et al. 1999b, Sakamoto, Baker & Scoville 2000, Sheth et al. 2000, Koda et al. 2002) yet NGC 3367 shows two large synchrotron lobes at either side of the center (at radius 6 kpc from the nucleus); a very similar outflow is observed in NGC 3079 [Koda et al. 2002]. No broad line region is observed in NGC 3367, very likely the result of high extinctions in the molecular gas. The optical disk of NGC 3367 is peculiar (García-Barreto, Franco & Carrillo 1996): (a) there is a bright optical structure forming a semi-circle at a radius of approximately $10 - 11 \text{ kpc}$ SW of the center; this structure is bright in optical red continuum as well as in narrow line $H\alpha + [\text{NII}]$ images; (b) it has spiral arms apparently joining this semi-circle structure (to the NW) at an angle larger

than 45° ; (c) the NW spiral arm seems to consist of two parallel structures (both in red images and in $H\alpha$ + $[NII]$ images); (d) the north-east (NE) end of the stellar bar exhibits very large velocity dispersions in $H\alpha$ Garcia-Barreto & Rosado 2001. Our previous analysis of the optical morphology suggested a ringlike density wave propagating outwards possibly the result of a collision of NGC 3367 with a smaller galaxy (García-Barreto, Franco & Carrillo 1996). The perturber might have traveled approximately perpendicular to the disk of NGC 3367 in an off-center collision. Simulations of such galaxy collisions indicate an arc-like density wave which propagates outwards from the point of impact (Lynds & Toomre 1976, Toomre 1978, Mihos & Hernquist 1994, Gerber, Lamb & Balsara 1996). In contrast to central collisions, the off-center collisions create elongated (non-circular) structures (Toomre 1978, Gerber & Lamb 1994). Another possible scenario for NGC 3367 might be a merger with a dwarf galaxy (Hernquist 1989) in which the dwarf is gradually tidally disrupted and its remains are distributed asymmetrically in the disk by differential rotation.

The **total** star formation rate can be crudely estimated from the bolometric luminosity using : $SFR \sim 8 \times 10^{-11} L_{TOT}/L_\odot M_\odot yr^{-1}$ (Scoville & Young 1983). For the observed luminosity of $L_{TOT} = L_B + L_{FIR} \sim 6.8 \times 10^{10} L_\odot$, we obtain $SFR \sim 5 M_\odot yr^{-1}$ which is similar to that of the Galaxy.

4.5. Other Galaxies with Similar Nuclear Characteristics

Other barred galaxies show bipolar synchrotron emission from their nucleus. Most notably, NGC 1068, (SBb, classified as Sy 2, and hidden Sy 1) has a synchrotron bipolar outflow from the nucleus ~ 950 pc in diameter (van der Hulst, Hummel & Dickey 1982, Ulvestad, Neff & Wilson 1987). NGC 3079 (SBc) has a synchrotron bipolar outflow out to a radius of ~ 1.2 kpc perpendicular to the plane of the disk (Duric & Seaquist 1988, Koda et al. 2002). NGC 5548 (S0a, classified as Sy 1) exhibits strong and variable X-ray emission and bipolar synchrotron emission; the bipolar emission diameter is only 4 kpc (Ho & Ulvestad 2001). Deep optical images of NGC 5548 show tidal tails suggesting a past merger (Tyson et al. 1998). NGC 5643, SABc (Sy 2), has a radio continuum and $H\alpha$ morphology elongated at the PA of the stellar bar. The radio continuum extension in NGC 5643 is about 1.7 kpc in diameter and the galaxy has no companions within $10 D_{25}$.

5. CONCLUSIONS

We have carried out interferometric (mm OVRO) observations of the CO (1-0) emission from the radio-bipolar lobe galaxy NGC 3367. The observations indicate that the molecular gas is concentrated in the central ($9''$) region with some weak emission from regions just beyond the ends of the (optical) stellar bar to the W and E sides.

The molecular gas mass is $3 \times 10^8 M_\odot$ in the central peak of the emission ($2.5 \times 1.45''$ or 525×300 pc) and $5.9 \times 10^8 M_\odot$ within a radius of $4''.5$ (950 pc). The high molecular gas mass in the center of the galaxy translates in an extremely large optical depth which is likely to block optical broad line emission from the AGN.

Our high angular resolution ($2.6 \times 1.9''$, FWHM) map of the central emission indicates an unresolved source at $\alpha = 10^h 46^m 34^s.948$, $\delta = +13^\circ 45' 02''.7$ which coincides with the

nuclear radio continuum peak ($\alpha = 10^h 46^m 34^s.956, \delta = +13^\circ 45' 02.94''$). In addition, we have detected emission extended from the central peak to the NE and SW. This is also the direction of the arc second extended synchrotron emission leading to the 12 kpc diameter lobes.

The velocity field of the central region indicates two peaks which we believe reflect the existence of a density decrease with the central 100 pc around the AGN. This clearing might result from either the AGN winds or more likely the gas dynamics at the inner Lindblad resonance.

Acknowledgements

We thank the staff of the Owens Valley Radio Observatory. The Owens Valley Millimeter Array is supported by the National Science Foundation (NSF) grant AST 99-81546. JAG-B would like to thank Nick Scoville and the Radio Astronomy Millimeter Group at Caltech for their hospitality during a six month visit where part of this paper was written and to DGAPA-UNAM (Mexico) for its partial financial support during his stay at Caltech. JAG-B would also like to thank the time allocating committee of the OVRO millimeter array for the allocated observing time for this project.

REFERENCES

- Antonucci, R. R. J. & Miller, J. S. 1985, *ApJ*, 297, 621
- Blandford, R. D. 1990 in *Active Galactic Nuclei, SAAS-FEE Advance Course 20*, Ed. T. J.-L. Courvoisier & M. Mayor (Berlin: Springer Verlag), p. 161 Wielebinski, R. & Brouiliet, N. 1993, *A&AS*, 97, 887
- Bridle, A. H. & Perley, R. A. 1984, *ARA&A*, 22, 319
- Buta, R., 1986, *ApJS*, 61, 639
- Buta, R. & Combes, F., 1996, *Fundam.Cosmic Phys.*, 17, 95
- Colbert, E. J. M., Baum, S. A., Gallimore, J. F., O’Dea, C. P., & Christensen, J. A. 1996, *ApJ*, 467, 551
- Contopoulos, G. & Grosbol, P., 1989 *A&ARv*, 1, 261
- Crane, P. C. & van der Hulst, J. M. 1992, *AJ*, 103, 1146
- Downes, D., Reynaud, D., Solomon, P.M. & Radford, S.J.E. 1996, *ApJ*, 461, 186
- Downes, D., Solomon, P.M. & Radford, S.J.E. 1993, *ApJ*, 414, L13
- Duric, N. & Seaquist, E.R. 1988, *ApJ*, 326, 574
- Fabbiano, G., Kim, D.-W., & Trinchieri, G. 1992, *ApJS*, 80, 531
- García-Barreto, J.A., Dettmar, R.-J, Combes, F., Gerin, M., Koribalski, B. 1991a, *Rev.Mex.Astron.Astrof.*, 22, 197
- García-Barreto, J.A., Downes, D., Combes, F., Gerin, M., Magri, C., Carrasco, L. & Cruz-Gonzalez, I. 1991b, *A&A*, 244, 257
- García-Barreto, J.A., Carrillo, R., Klein, U. & Dahlem, M. 1993, *Rev.Mex.Astron.Astrof.* 25, 31
- García-Barreto, J.A., Carrillo, R. & Vera-Villamizar, N. 2003, *AJ*, 126, 1707.
- García-Barreto, J.A., Franco, F., & Carrillo, R. 1996, *ApJ*, 469, 138
- García-Barreto, J.A., Franco, F., Carrillo, R., Venegas, S.& Escalante-Ramírez, B. 1996, *Rev.Mex. Astron. Astrofis.*, 32, 89
- García-Barreto, J.A., Franco, F., & Rudnick, L. 2002, *AJ*, 123, 1913
- García-Barreto, J.A. & Rosado, M. 2001, *AJ*, 121, 2540
- García-Barreto, J.A., Rudnick, L., Franco, F., & Martos, M. 1998, *AJ*, 116, 111
- Gerber, R. A. & Lamb, S. A. 1994, *ApJ*, 431, 604
- Gerber, R. A., Lamb, S. A. & Balsara, D. S. 1996, *MNRAS*, 278, 345
- Grosböl, P.J. 1985, *A&AS*, 60,261

- Henriksen, R. N., Vallée, J. P. & Bridle, A. H. 1981, *ApJ*, 249, 40
- Hernquist, L. 1989, *Nature*, 340, 687
- Ho, L.C., Filippenko, A.V. & Sargent, W.L.W. 1995, *ApJS*, 98, 477
- Ho, L.C., Filippenko, A.V. & Sargent, W.L.W. 1997, *ApJS*, 112, 315
- Ho, L.C., & Ulvestad, J. S. 2001, *ApJS*, 133, 77
- Huchtmeier, W.K. & Richter, O.-G. 1989, *A General Catalog of HI Observations* (New York: Springer Verlag)
- Huchtmeier, W.K. & Seiradakis, J. H. 1985, *A&A*, 143, 216
- Kinney, A.L., Schmitt, H. R., Clarke, C. J., Pringle, J.E., Ulvestad, J. S. & Antonucci, R. R. J. 2000, *ApJ*, 537, 152
- Koda, J., Sofue, Y., Kohno, K., Nakanichi, H., Onodera, S., Okumura, S. K. & Irwin, J. A. 2002, *ApJ*, 573, 105
- Lynds, R. & Toomre, A. 1976, *ApJ*, 209, 382
- Mihos, J.C. & Hernquist, L. 1994, *ApJ*, 437, 611 216, 193
- Pringle, J.E., Antonucci, R.R.J., Clarke, C.J., Kinney, A.L., Schmitt, H.R. & Ulvestad, J.S. 1999, *ApJ*, 526, L9
- Regan, M.W., Sheth, K., & Vogel, S.N. 1999, *ApJ*, 526, 97
- Reynaud, D. & Downes, D. 1997, *A&A*, 319, 737
- Reynaud, D. & Downes, D. 1998, *A&A*, 337, 671
- Sakamoto, K., Baker, A. & Scoville, N. Z. 2000, *ApJ*, 533, 149
- Sakamoto, K., Okumura, S.K., Ishizuki, S. & Scoville, N. Z. 1999a, *ApJS*, 124, 403
- Sakamoto, K., Okumura, S.K., Ishizuki, S. & Scoville, N. Z. 1999b, *ApJ*, 525, 691
- Sandage, A. & Tamman, G.A. 1981, *A Revised Shapley Ames Catalog of Bright Galaxies*, Washington: Carnegie Institution of Washington, publication 635.
- Schinnerer, E., Eckart, A., Tacconi, L. J., Genzel, R. & Downes, D. 2000, *ApJ*, 533, 850
- Scoville, N.Z., Carlstrom, J.E., Chandler, C.J., Phillips, J.A., Scott, S.L., Tilanus, R.P.J. & Wang, Z. 1993, *PASP*, 105, 1482
- Scoville, N.Z. & Young, J.S. 1983, *ApJ*, 265, 148
- Scoville, N.Z., Yun, M.S. & Bryant, P.M. 1997, *ApJ*, 484, 702
- Sheth, K., Regan, M.W., Vogel, S.N., & Teuben, P.J., 2000, *ApJ*, 532, 221
- Sheth, K., Vogel, S.N., Regan, M.W., Teuben, P.J., Harris, A.I., & Thornley, M.D. 2002, *AJ*, 124, 2581

- Sheth, K., Vogel, S.N., Regan, M.W., Teuben, P.J., Harris, A.I., Thornley, M.D. & Helfer, T.T. 2004, in preparation
- Soifer, B. T., Bohemer, L., Neugebauer, G. & Sanders, D. B. 1989, *AJ*, 98, 766
- Toomre, A. 1978 in *The Large Scale Structure of the Universe*, ed. M. S. Longair & J. Einasto (Dordrecht: Reidel), 109
- Tully, R.B. 1988, *Nearby Galaxies Catalog, T88*, (Cambridge: Cambridge Univ. Press).
- Tyson, J.A., Fischer, P., Guhathakurta, P., McIlroy, P., Wenk, P. Huchra, J., Lucas, M., Neuschaefer, L., Sarajedini, V., Glazebrook, K., Ratnatunga, K. & Griffiths, R. 1998, *AJ*, 116, 102
- Ulvestad, J. S., Neff, S. G. & Wilson, A. S. 1987, *AJ*, 92, 22
- van der Hulst, J. M., Hummel, E. & Dickey, J. M. 1982, *ApJ*, 261, L 59 2001, *ApJ*, 547, 187
- Véron, P., Goncalves, A.C. & Véron-Cetty, M. P. 1997, *A&A*, 319, 52
- Véron-Cetty, M.P. & Véron, P. 1986, *A&AS*, 66, 335
- Véron-Cetty, M.P. & Véron, P. 1996 *A Catalog of Quasars and Active Nuclei*, 7th. Edition (Garching bei München: ESO)
- Wilson, A. S. & Ulvestad, J.S., 1987 *ApJ*, 319, 105
- Young, J. S., Scholerb, F. P., Kenney, J.D. & Lord, S.D. 1986, *ApJ*, 304, 443
- Young, J.S. & Scoville, N.Z. 1982, *ApJ*, 258, 467

Table 1: Barred Spiral Galaxy NGC 3367

| Property | | Reference |
|---|------------------------------|-----------|
| Hubble Type | SBc(s) | 1 |
| Right Ascension (J2000) | $10^h 46^m 34^s.956$ | 2 |
| Declination (J2000) | $+13^\circ 45' 2''.94$ | 2 |
| Distance | 43.6 Mpc | 3 |
| Optical Diameter | 2'.5 | 3 |
| Log L_B | 10.68 | 3 |
| Optical Classification | HII, Sy 2-like | 4 |
| M(HI) | $7 \times 10^9 M_\odot$ | 5 |
| $V_{Systemic}(\text{HI})$ | 3030 km s^{-1} | 5 |
| Far Infrared Luminosity (IRAS) | $2.1 \times 10^{10} L_\odot$ | 6 |
| Star Formation Rate | 5 | 7 |
| Position Angle Disk | 109° | 8 |
| Dust Temperature (IRAS) | 34° K | 9 |
| Stellar Bar diameter | $32''$ (6.7 kpc) | 9 |
| PA Bar | 65° | 9 |
| Inclination | 30° | 10 |
| Tully's Group | 32-4+4 | 3 |
| Nearby Companions within 10 D ₂₅ | 0 | 11 |
| Nearby Companions between 10 D ₂₅ and 20 D ₂₅ | 1 | 11 |

References: 1) Sandage & Tamman (1981); 2) Garcia-Barreto et al. (2002); 3) Tully (1988); 4) Veron-Cetty & Veron (1986,1996); 5) Huchtmeier & Seiradakis (1985); 6) Soifer et al. (1989); 7) $\dot{M}_{OBA} \sim 7.7 \times 10^{-11} L_{TOT}/L_\odot M_\odot \text{ yr}^{-1}$ [Scoville & Young (1983)]; for NGC 3367, $L_{TOT} = L_B + L_{FIR} L_{TOT} \sim 6.8 \times 10^{10} L_\odot$; 8) Grosböl (1985); 9) Garcia-Barreto et al. (1993,1996b); 10) Garcia-Barreto & Rosado (2001); 11) Garcia-Barreto, Carrillo & Vera-Villamizar (2003)

Table 2: CO(1-0) Parameters

| | |
|---|--|
| Phase center α (J2000) | $10^h 46^m 34^s.95$ |
| Phase center δ (J2000) | $+13^\circ 45' 3''$ |
| FWHM low resolution | $4''.26 \times 2''.71$, PA= 176° |
| FWHM high resolution | $2''.63 \times 1''.94$ PA= 96° |
| Primary beam diameter | 10.4 m |
| Primary beam (FWHM) | $53''$ at 114.1 GHz |
| 1 σ rms noise in channel maps | 6 mJy / beam |
| 1 σ rms noise in high resolution maps | 150 mJy / km s $^{-1}$ |
| 1 σ rms noise in low resolution maps | 200 mJy / km s $^{-1}$ |
| M(H $_2$) peak ($2''.5 \times 1''.4$) | $3 \times 10^8 M_\odot$ |
| M(H $_2$) within $r=4''.5$ ($r \leq 950$ pc) | $5.9 \times 10^8 M_\odot$ |
| M(H $_2$) within $r=27''$ ($r \leq 5.7$ kpc) | $2.6 \times 10^9 M_\odot$ |
| H $_2$ surface density at $R \leq 950$ pc | $\sim 210 M_\odot \text{ pc}^{-2}$ |
| H $_2$ surface density at $R \leq 200$ pc | $\sim 2.5 \times 10^3 M_\odot \text{ pc}^{-2}$ |
| Beam average N(H $_2$) at $R \leq 200$ pc | $\sim 1.5 \times 10^{23} \text{ cm}^{-2}$ |
| Beam average N(H $_2$) at $R \leq 950$ pc | $\sim 1.3 \times 10^{22} \text{ cm}^{-2}$ |
| Beam average n(H $_2$) [N(H $_2$)/ l ; $l \sim 50$ pc] | $\sim 950 \text{ cm}^{-3}$ |
| Beam average n(H $_2$) [N(H $_2$)/ l ; $l \sim 50$ pc] | $\sim 85 \text{ cm}^{-3}$ |
| Visual Extinction ^a , $A_v(1)$, towards nucleus | 150 mag |
| Star Formation Rate ^b , | $\sim 5 M_\odot \text{ yr}^{-1}$ |

(a) $N(\text{H}_2)/A_v = 0.94 \times 10^{21} \text{ cm}^{-2} \text{ mag}^{-1}$ (Young & Scoville 1982); (b) $\sim 8 \times 10^{-11} L_{TOT}$ (Scoville & Young 1983).

6. FIGURE CAPTIONS

Figure 1. Spectrum of CO(1-0) emission in NGC 3367 from low resolution (fwhm $4''.2 \times 2''.7$ beam) data smoothed to 15.9 km/s is shown for a $17''.5$ (1.8 kpc radius) aperture centered on the nucleus in NGC 3367. The systemic velocity of the galaxy, $V_{sys} \approx 3032$ km s⁻¹ is from H α Fabry-Perot.

Figure 2. CO (1-0) (FWHM $4.2 \times 2.7''$ beam) channel maps (twenty channels covering 300 km s⁻¹) in contours superimposed on the optical continuum I image (Garcia-Barreto et al. 1996a,1996b). Contours are at -3,3,4,5,6,7,8,9,10,15,20 \times 6 mJy/beam.

Figure 3. CO(1-0) integrated line flux over 300 km s⁻¹ with low angular resolution (beam FWHM $4''.2 \times 2''.7$) superimposed on the greyscale H α + [NII] image (Garcia-Barreto et al. 1996a,1996b). CO contours are at -3, 3, 5, 7, 9, 12, 14, 16, 18, 20, 22, 24, 26, 28, 30, 35, 40, 45, 50, 60, 70 \times 150 mJy km s⁻¹. The weak emission structure aligned north-south in the western side of the galaxy seems to originate from beyond the stellar bar. The unresolved source seems to originate from the expected location of dust lane in the stellar bar, that is, from the north-western side of the stellar bar assuming the bar is rotating counter clockwise (with the assumption of trailing spiral arms).

Figure 4. CO(1-0) integrated line flux over 300 km s⁻¹ with low angular resolution (beam FWHM $4.2 \times 2.7''$) superimposed on the optical continuum greyscale I image (Garcia-Barreto et al. 1996a,1996b). Contours are at -3, 3, 5, 7, 9, 12, 14, 16, 18, 20, 22, 24, 26, 28, 30, 35, 40, 45, 50, 60, 70 \times 150 mJy km s⁻¹. Weak emission is detected from the NNW and SNE sides of the ends of the stellar bar.

Figure 5. High angular (FWHM $2.6 \times 1.9''$) resolution CO(1-0) integrated line flux over 300 km s⁻¹ (in grey scale and contours). Peak of the CO emission is at $\alpha(J2000) = 10^h 46^m 34^s .948$, $\delta(J2000) = +13^\circ 45' 02''.7$. Secondary peak to the south-west is at $\alpha(J2000) = 10^h 46^m 34^s .66$, $\delta(J2000) = +13^\circ 45' 0.90''$. Contours are at -3, 3, 5, 7, 9, 12, 14, 16, 18, 22, 26, 30, 35, 40, 45, 50, 55, 60, 70, 75 \times 150 mJy km s⁻¹. The main CO peak position is to be compared with the peak of the high resolution synchrotron emission at $\alpha(J2000) = 10^h 46^m 34^s .956$, $\delta(J2000) = +13^\circ 45' 02''.94$ (see Fig. 10).

Figure 6. CO centroid velocities in contours superposed on the integrated CO line flux in grayscale. The CO systemic velocity is $V_{sys} \sim 3035$ km s⁻¹.

Figure 7. Dispersion velocity map (moment 2) from the central region of NGC 3367 using the low resolution map (grey scale and contours). Large velocity dispersion is detected in the central region in PA40 $^\circ$ which corresponds to the kinematical minor axis of NGC 3367. Dispersion velocity of $\sigma_v \sim 40/\sin i$ km s⁻¹ is detected from the NW which would correspond to the crossing of the x_1 and x_2 orbits from the main stellar bar. The largest dispersion, however, is $\sigma_v \sim 75/\sin i$ km s⁻¹ in the region $\alpha = 34^s .66$; $\delta = 45' 00''.90$ which corresponds to a region with weak or no radio continuum synchrotron emission (see Fig. 11 this paper and Fig. 2 in Garcia-Barreto, Franco & Rudnick 2002).

Figure 8. Position-velocity diagram from the high resolution map (beam $2''.6 \times 1''.9$) obtained by adding the emission within $\pm 2''$ of the major axis (PA=51 $^\circ$). The distance between two ticks along the major axis corresponds to 735 kpc. The blue shifted velocity (primary) peak is at 3022 km s⁻¹ while the red shifted velocity (secondary) peak is at 3068

km s⁻¹; their separation is 110 pc.

Figure 9. Reproduction of the innermost 3'' radio continuum image at 8.4 GHz (in grey scale and contours). Peak of the radio continuum emission (at an angular resolution of 0''.28 × 0''.25) is at $\alpha(J2000) = 10^h46^m34^s.956$, $\delta(J2000) = +13^\circ45'02''.94$ (Garcia-Barreto et al. 2002). This position is compared to the position of the high resolution CO peak of emission at $\alpha(J2000) = 10^h46^m34^s.948$, $\delta(J2000) = +13^\circ45'02''.7$ (see Fig. 5)

Figure 10. Reproduction of the innermost 7'' radio continuum image with 1.4 GHz (in contours) and 8.4 GHz (in grey scale, Garcia-Barreto et al. 2002)

Figure 11. Reproduction of the large scale radio continuum image with optical *I* optical continuum emission (in contours) and 1.4 GHz radio continuum emission (in grey scale, García-Barreto, Franco & Rudnick 2002). Notice the large scale lobes straddling the center at a projected radius of 6 kpc.

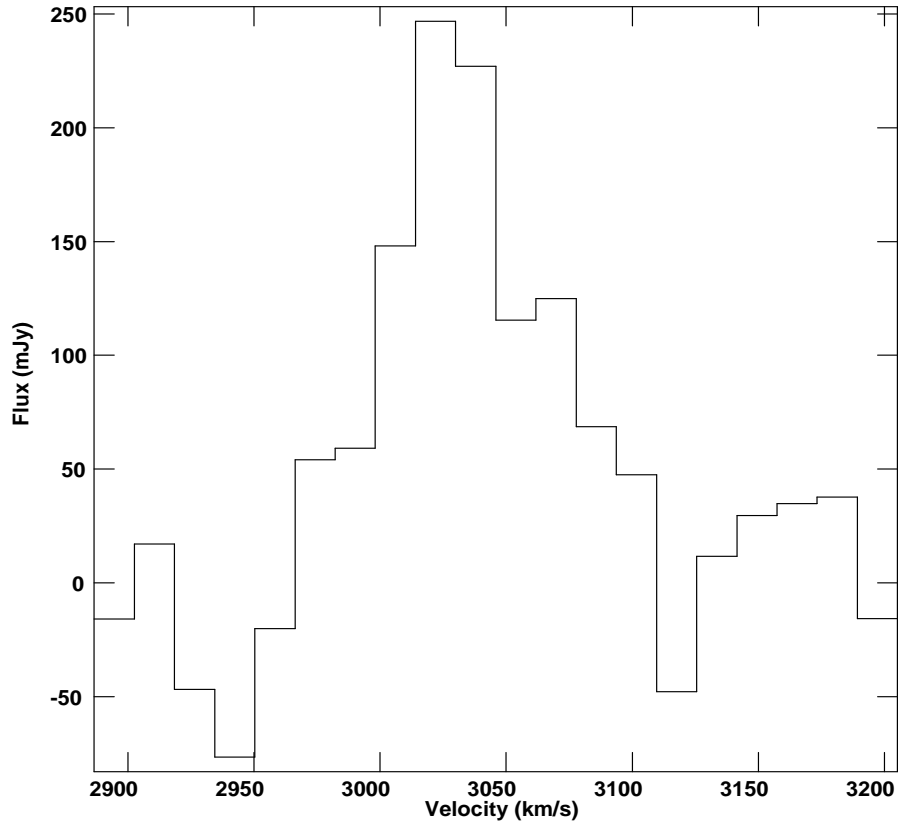


Fig. 1.— Spectrum of CO(1-0) emission in NGC 3367 from low resolution (fwhm $4''.2 \times 2''.7$ beam) data smoothed, in velocity, to 15.9 km/s is shown for a $17''.5$ (1.6 kpc radius) aperture centered on the nucleus in NGC 3367. The systemic velocity of the galaxy, $V_{sys} \approx 3032$ km s $^{-1}$ is from H α Fabry-Perot (Garcia-Barreto & Rosado 2001).

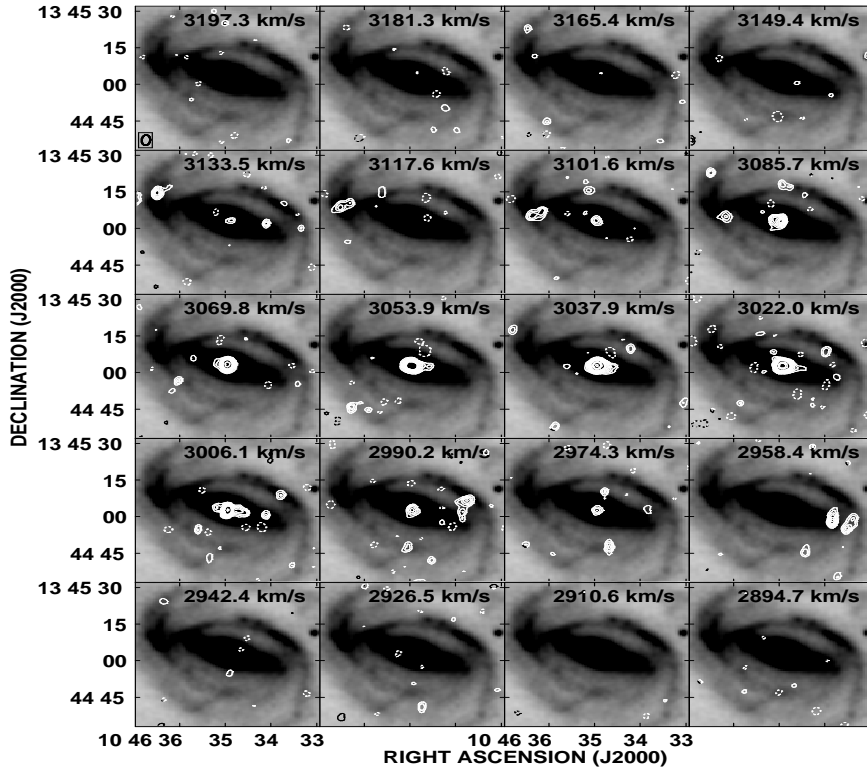


Fig. 2.— CO (1-0) (fwhm $4''.2 \times 2''.7$ beam) channel velocity maps (twenty channels covering about 300 km s^{-1}) in contours superimposed on the optical continuum I image (Garcia-Barreto et al. 1996a,1996b). Contours are in units of 6 mJy/beam and are - 3,3,4,5,6,7,8,9,10,15,20.

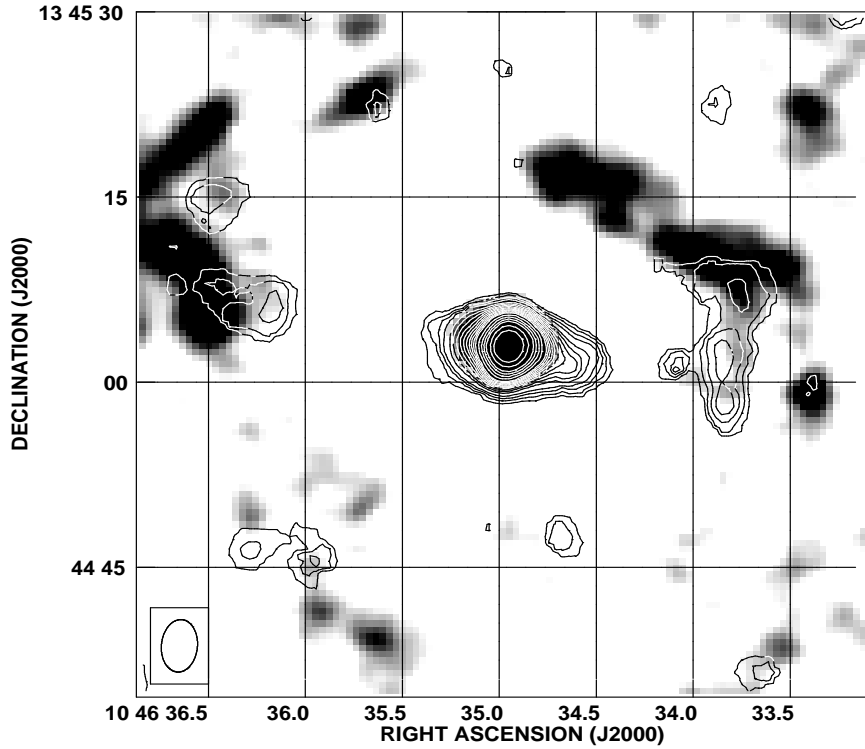


Fig. 3.— CO(1-0) integrated line flux over 300 km s^{-1} with low angular resolution (beam FWHM $4''.2 \times 2''.7$) superimposed on the greyscale $\text{H}\alpha + [\text{NII}]$ image (Garcia-Barreto et al. 1996a, 1996b). CO contours are in units of $0.15 \text{ Jy km s}^{-1}$ and are -3, 3, 5, 7, 9, 12, 14, 16, 18, 20, 22, 24, 26, 28, 30, 35, 40, 45, 50, 60, 70. The weak emission structure aligned north-south in the western side of the galaxy seems to originate from beyond the stellar bar. The unresolved source seems to originate from the expected location of dust lane in the stellar bar, that is, from the north-western side of the stellar bar assuming the bar is rotating counter clockwise (with the assumption of trailing spiral arms).

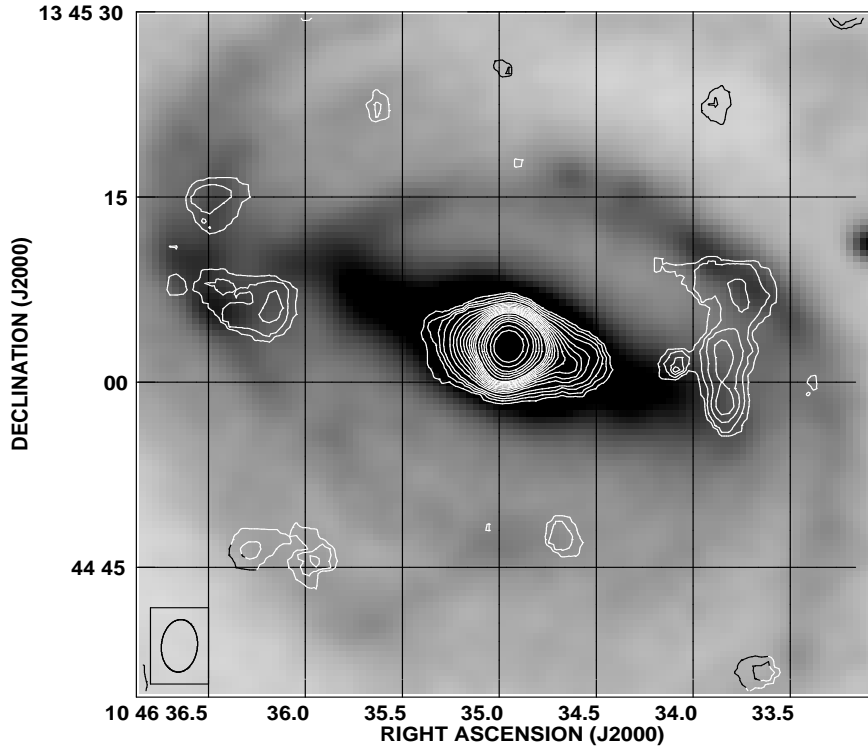


Fig. 4.— CO(1-0) integrated line flux over 300 km s^{-1} with low angular resolution (beam FWHM $4''.2 \times 2''.7$) superimposed on the optical continuum greyscale I image (Garcia-Barreto et al. 1996a,1996b). Contours are in units of $0.15 \text{ Jy km s}^{-1}$ and are -3, 3, 5, 7, 9, 12, 14, 16, 18, 20, 22, 24, 26, 28, 30, 35, 40, 45, 50, 60, 70. Weak emission is detected from the NNW and SNE sides of the ends of the stellar bar.

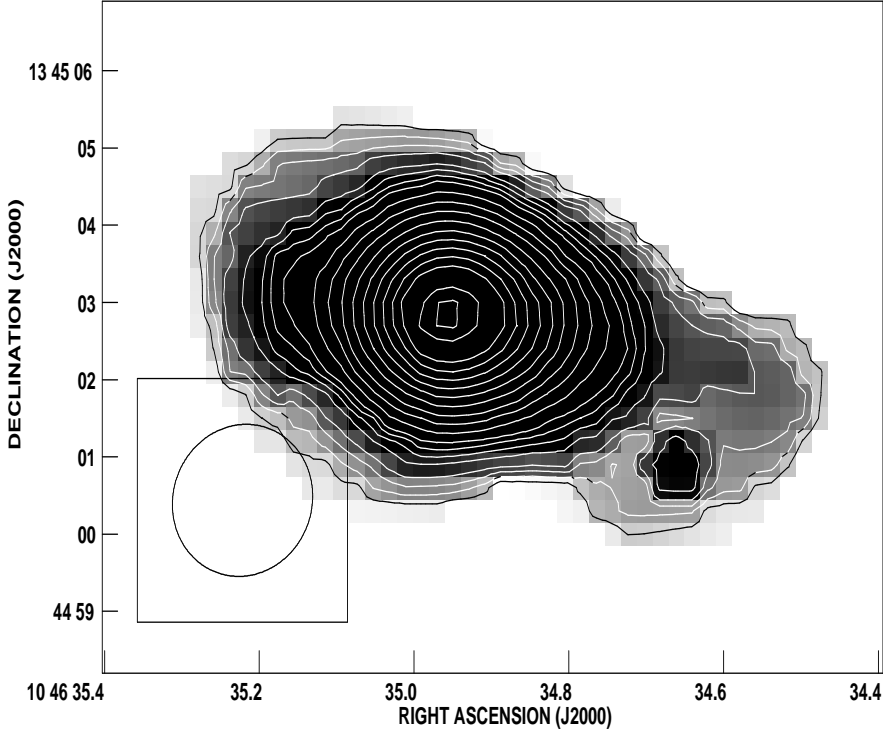


Fig. 5.— High angular (FWHM $2''.6 \times 1''.9$) resolution CO(1-0) integrated line flux over 300 km s^{-1} (in grey scale and contours). Peak of the CO emission is at $\alpha(J2000) = 10^h 46^m 34^s.948$, $\delta(J2000) = +13^\circ 45' 02''.7$. Secondary peak to the south-west is at $\alpha(J2000) = 10^h 46^m 34^s.66$, $\delta(J2000) = +13^\circ 45' 00''.90$. Contours are in units of $0.15 \text{ Jy km s}^{-1}$ and are -3, 3, 5, 7, 9, 12, 14, 16, 18, 22, 26, 30, 35, 40, 45, 50, 55, 60, 70, 75. The main CO peak position is to be compared with the peak of the high resolution synchrotron emission at $\alpha(J2000) = 10^h 46^m 34^s.956$, $\delta(J2000) = +13^\circ 45' 02''.94$ (see Fig. 10).

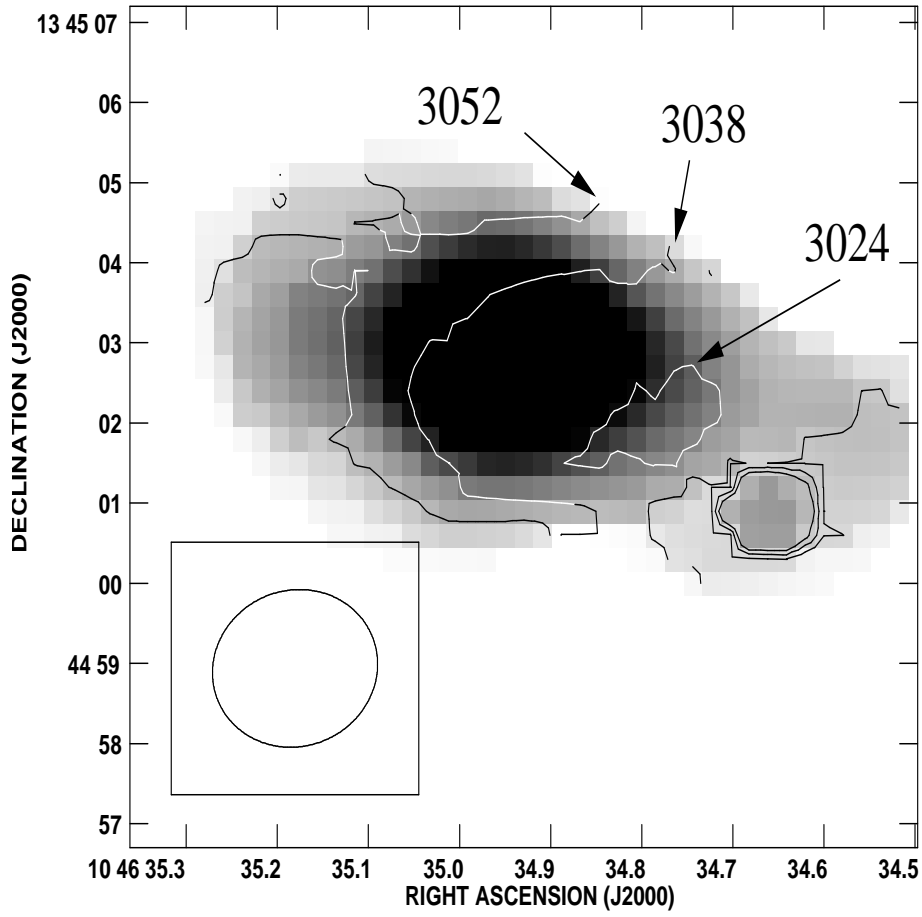


Fig. 6.— CO centroid velocities in contours superposed on the integrated CO line flux in grayscale. The CO systemic velocity is $V_{sys} \sim 3035 \text{ km s}^{-1}$.

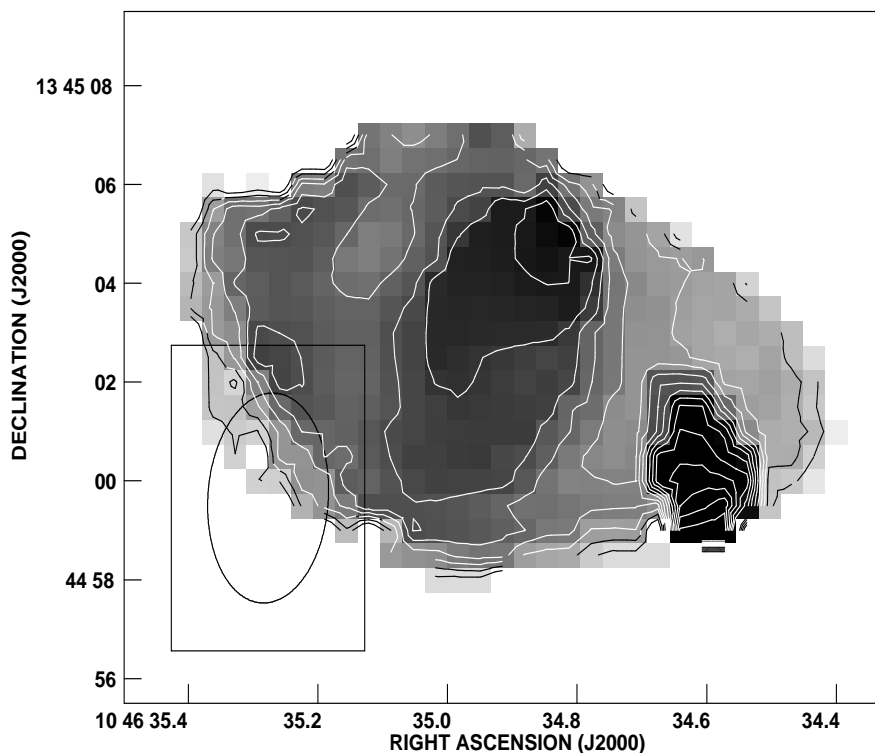


Fig. 7.— Dispersion velocity map (moment 2) from the central region of NGC 3367 using the low resolution map (grey scale and contours). Large velocity dispersion is detected in the central region in PA40° which corresponds to the kinematical minor axis of NGC 3367. Dispersion velocity of $\sigma_v \sim 40/\sin i$ km s⁻¹ is detected from the NW which would correspond to the crossing of the x_1 and x_2 orbits from the main stellar bar. The largest dispersion, however, is $\sigma_v \sim 75/\sin i$ km s⁻¹ in the region $\alpha = 34^s.66$; $\delta = 45'00''.90$ which corresponds to a region with weak or no radio continuum synchrotron emission (see Fig. 11 this paper and Fig. 2 in Garcia-Barreto, Franco & Rudnick 2002).

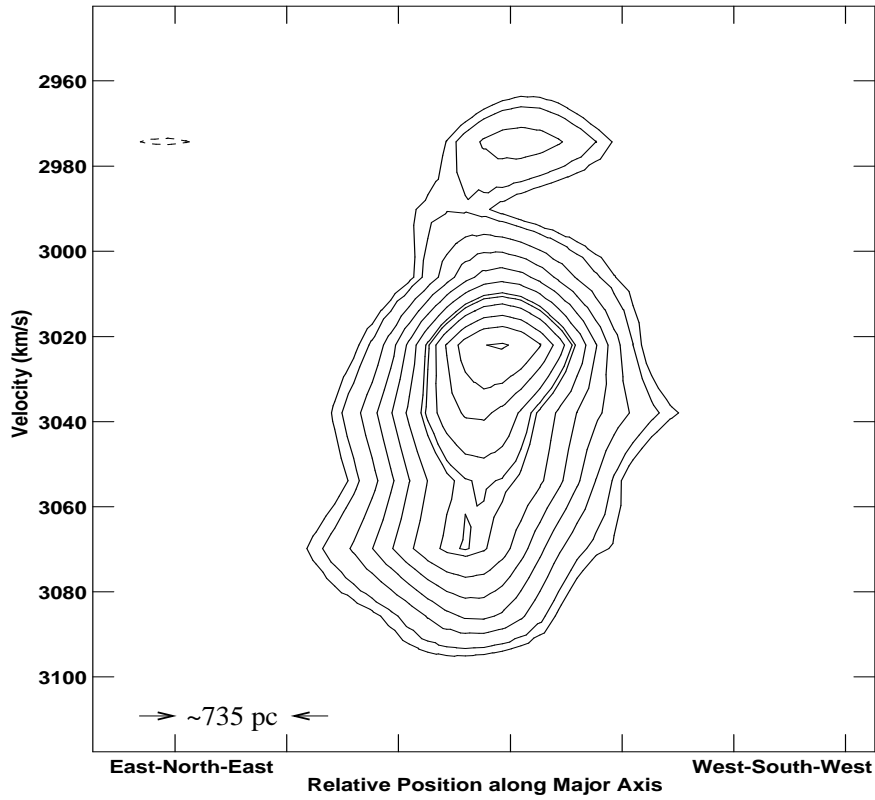


Fig. 8.— Position-velocity diagram from the high resolution map (beam $2''.6 \times 1''.9$) obtained by adding the emission within $\pm 2''$ of the major axis (PA= 51°). The distance between two ticks along the major axis corresponds to ~ 735 pc. The blue shifted velocity (primary) peak is at 3022 km s^{-1} while the red shifted velocity (secondary) peak is at 3068 km s^{-1} ; their separation is 110 pc.

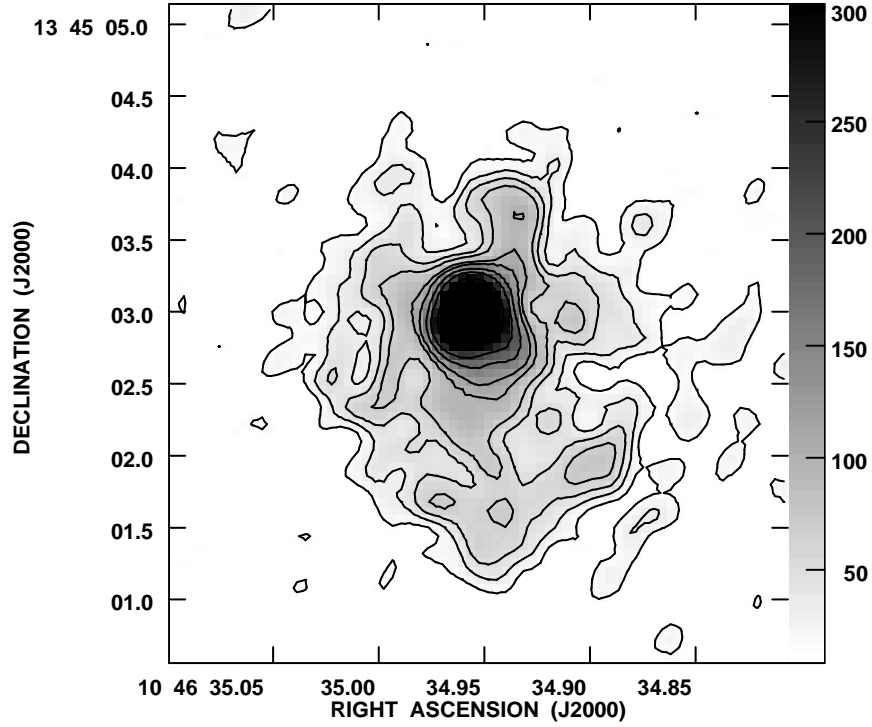


Fig. 9.— Reproduction of the innermost 3'' radio continuum image at 8.4 GHz (in grey scale and contours). Peak of the radio continuum emission (at an angular resolution of $0''.28 \times 0''.25$) is at $\alpha(J2000) = 10^h46^m34^s.956$, $\delta(J2000) = +13^\circ45'02''.94$ (Garcia-Barreto et al. 2002). This position is compared to the position of the high resolution CO peak of emission at $\alpha(J2000) = 10^h46^m34^s.948$, $\delta(J2000) = +13^\circ45'02''.7$ (see Fig. 5).

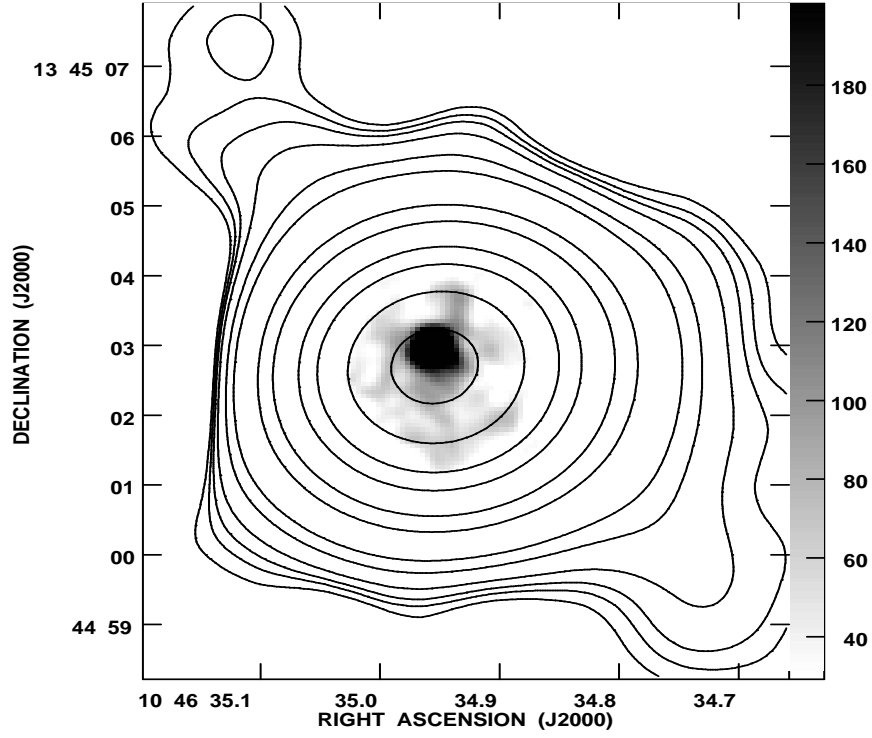


Fig. 10.— Reproduction of the innermost 7'' radio continuum image with 1.4 GHz in contours and 8.4 GHz in grey scale (García-Barreto, Franco & Rudnick 2002)

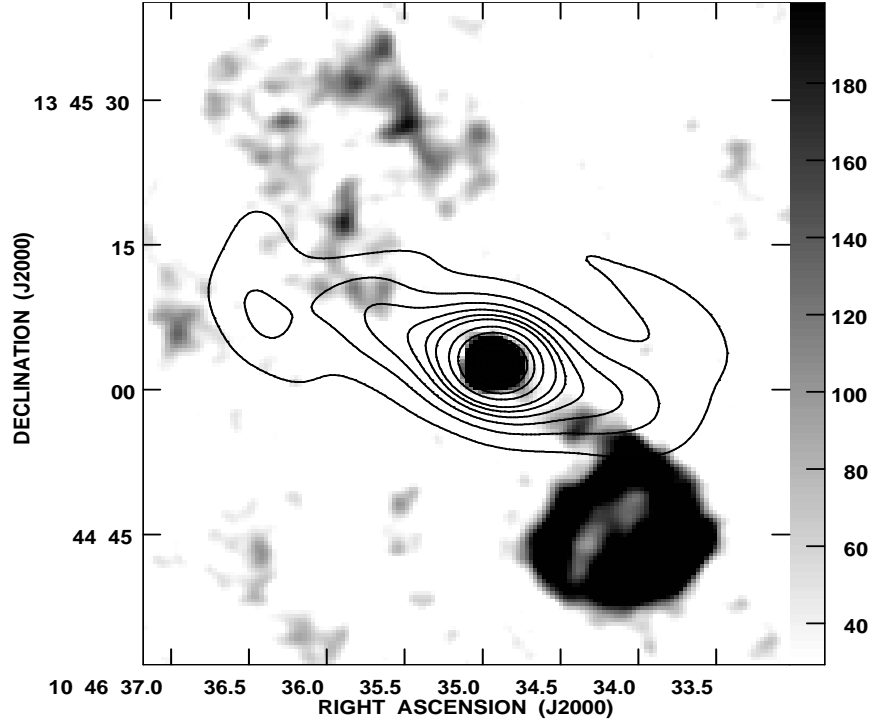


Fig. 11.— Reproduction of the large scale radio continuum 1.4 GHz emission image (in grey scale) superposed to optical *I* continuum emission (in contours; García-Barreto, Franco & Rudnick 2002). Notice the large scale lobes straddling the center at a projected radius of 6 kpc.